Numerical Solution of the Stationary State Schrödinger Equation Using Transparent Boundary Conditions

To solve the discrete version of the stationary state Schrödinger equation to Numerov accuracy, the author uses boundary conditions at the limits of the computational domain that mimic an interval of infinite extent. He also describes methods for finding particle energies, scattering coefficients, and partial-wave phase shifts.

Eigenvalue problems in the form of differential equations have widespread application in all fields of science and engineering. Their numerical study requires replacing the continuum formulation with a discrete version, then solving the resulting model iteratively using appropriate start values. How to choose start values in each individual case is a matter of some controversy.

In this article, I advocate using discrete transparent boundary conditions (DTBCs), a technique that has proven successful in other contexts. Implementing DTBCs for eigenvalue problems typically involves an approximation—the slowly varying approximation—that I present here along with suitable criteria for its validity. As the examples make clear, this approach isn't limited to just finding eigenvalues but also can be adapted to calculate other properties of physical interest.

Background

Schrödinger's equation for the stationary states of a particle with mass m in a 1D potential $V(x)$,

$$-\frac{\hbar^2}{2m}\frac{d^2\psi_E}{dx^2} + V(x)\psi_E(x) = E\psi_E(x)\,,$$

is an example of an eigenvalue problem. The coordinate x extends from $-\infty$ to $+\infty$, and acceptable waveforms $\psi_E(x)$ must be continuous bounded functions of x, which are conditions that generally occur only for special values of the particle energy E. The eigenvalues are these allowed energies, and the corresponding eigenfunctions are the stationary states $\psi_E(x)$.

For simplicity, we can recast the problem as

$$\frac{d^2y}{dx^2} + g(x)y(x) = 0\,. \qquad (1)$$

The stationary state Schrödinger equation is recovered with the obvious identifications $y(x) = \psi_E(x)$ and $g(x) = 2m[E - V(x)]/\hbar^2$. The discrete version of this equation follows by writing $x \to x_n \equiv nh$ and $f(x) \to f(x_n) \equiv f_n$ for any function $f(x)$, where n is an integer and h is the size of the spatial grid. The procedure would be straightforward except for the second derivative, which requires some approximation. To this end, note that

$$\Delta^2 f_{n-1} = \Delta(\Delta f_{n-1}) = f(x_n + h) + f(x_n - h) - 2f(x_n),$$

where $\Delta f_{n-1} \equiv f_n - f_{n-1}$ symbolizes the usual forward

1521-9615/06/$20.00 © 2006 IEEE
Copublished by the IEEE CS and the AIP

Curt A. Moyer
University of North Carolina, Wilmington

difference operation on any function $f(x)$. Expanding the first two terms on the right in a Taylor series gives

$$\Delta^2 f_{n-1} = h^2 f''(x_n) + (h^4/12) f^{(iv)}(x_n) + O(h^6).$$

The simplest approximation $\Delta^2 f_{n-1} \approx h^2 f''(x_n)$ gives the central difference approximation to the second derivative and yields a discrete version of Equation 1 that is accurate to $O(h^3)$:

$$\Delta^2 y_{n-1} + h^2 g_n y_n = 0. \tag{2}$$

The Numerov method improves on this by using the original differential equation for $y(x)$ to write $h^2 f^{(iv)}(x_n) = -h^2 (gy)'' \approx -\Delta^2 [g_{n-1} y_{n-1}]$. This gives the Numerov discretization of Equation 1:

$$\Delta^2 \left[\left(1 + \frac{h^2}{12} g_{n-1} \right) y_{n-1} \right] + h^2 g_n y_n = 0 \,, \tag{3}$$

which is accurate to $O(h^5)$. Interestingly, the Numerov version is identical to Equation 2, with the replacements

$$y_n \to \left(1 + \frac{h^2}{12} g_n \right) y_n, \quad g_n \to \frac{g_n}{1 + \frac{h^2}{12} g_n} \,, \tag{4}$$

so the Numerov method's improved accuracy comes at negligible computational cost. For the remainder of this article, I will adopt Equation 2 as the discrete equation of interest, with the assurance that the results apply equally well to the Numerov version after suitably redefining the terms.

We can solve Equation 2 recursively, using given values for y_n at two successive points. Numerical stability requires that in regions in which $y(x)$ is monotonic, recursion should be performed in the direction of increasing $|y|$ to reduce the solution's relative error.[1] Oftentimes, this means constructing separate solutions starting from each interval limit, then matching them at some intermediate location. In any event, start values for each recursive solution must be known to an accuracy compatible with the algorithm we use. Obtaining those values in practical applications has sparked much discussion. Of course, $y_n = y(x_n)$ are immediately available if $y(x)$ is known exactly in the neighborhood of the interval limits, but such is rarely the case.

A less restrictive alternative was developed by J.L.M. Quiroz Gonzalez and D. Thompson,[2] who showed how to select start values up to Numerov accuracy by using the exact solution function $y(x_0)$ and its slope $y'(x_0)$ at a single endpoint x_0. But those values, too, are often elusive.

Here, I advocate a different approach: instead of focusing on the exact solution $y(x)$, we can recover start values from the asymptotic solutions to the discrete equation for y_n. This tactical shift amounts to fully embracing the discrete formulation for all values of n; in effect, we impose boundary conditions at the limits of the computational domain that mimic an interval of infinite extent. Researchers pioneered using such DTBCs in connection with solving the time-dependent Schrödinger equation;[3–5] applying DTBCs to stationary state problems is actually simpler, as we will see in the following sections. Although the technique is familiar,[6] its connection to DTBCs and a rigorous exposition of the related slowly varying approximation are new here.

Discrete Asymptotic Forms

If the computational domain corresponds to $N_1 \le n \le N_2$, then $-\infty < n < N_1$ and $N_2 < n < \infty$ define the *exterior regions*. Our task is to find suitable analytic solutions to Equation 2 in these exterior regions, from which we will infer the proper boundary conditions to be imposed at the limits of the actual (finite) computational interval. Because the exterior regions include the asymptotic realm $n \to \pm\infty$, solutions here can't diverge for large $|n|$ if they're to be physically acceptable.

Let's introduce the discrete counterpart of the logarithmic derivative of $y(x)$, $\mu_n \equiv \Delta y_n / y_{n+1}$, and a measure of its variability, $\Delta\mu_{n-1} = \mu_n - \mu_{n-1}$. In terms of these, Equation 2 becomes

$$\mu_n^2 + (h^2 g_n + \Delta\mu_{n-1})(1 - \mu_n) = 0 \,. \tag{5}$$

Throughout each exterior region, we assume for now that g_n is unchanged from its value at the inner boundary, g_{N_1} or g_{N_2}. But if g_n doesn't change, then neither does μ_n, so $\Delta\mu_{n-1}$ vanishes identically and Equation 5 reduces to a quadratic form that we can solve to give the root pair

$$\mu_n^{\pm} = \frac{1}{2} \left(h^2 g_n \pm \sqrt{h^4 g_n^2 - 4 h^2 g_n} \right) \tag{6}$$

with the property

$$(1 - \mu_n^+)(1 - \mu_n^-) = 1 \,. \tag{7}$$

(The index n is superfluous here, but I retain it for its usefulness in subsequent analysis.)

For $g_n < 0$ (or $h^2 g_n > 4$), both roots of Equation 6 are real. Because $(1 - \mu_n) y_{n+1} = y_n$, we must select the

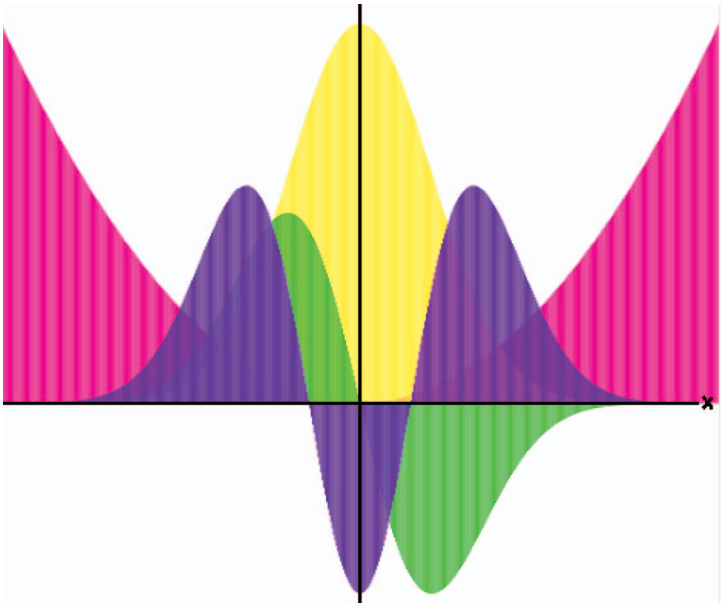

Figure 1. Some stationary state waveforms of the quantum oscillator, against the backdrop of the oscillator potential. The lowest energy wave (yellow) is nodeless, followed in order of energy by the wave with one node (green), two nodes (violet), and so forth. Because the energies are accurate, no discontinuity is evident in these waveforms.

root that makes $|y_{n+1}| > |y_n|$ over the left exterior region ($-\infty < n < N_1$) and $|y_{n+1}| < |y_n|$ on the right ($N_2 < n < \infty$) to generate solutions that approach zero as $n \to \pm\infty$. If $0 < h^2 g_n < 4$, then $\mu_n^{\pm}$ are complex conjugates, and Equation 7 implies $|1 - \mu_n^{\pm}| = 1$. It follows that the exterior solutions have constant modulus, $|y_{n+1}| = |y_n|$, and are oscillatory. Specifically, we have for this case $y_{n+1} = \exp(\pm i\theta_n) \cdot y_n$, where

$$\theta_n = \arctan\left(\frac{\sqrt{4h^2 g_n - h^4 g_n^2}}{|2 - h^2 g_n|}\right). \quad (8)$$

The preceding analysis leads us to the following algorithm for constructing stationary states:

1. If $g_{N_1} < 0$, take $y_{N_1+1} = (1 - \mu_{N_1})^{-1} y_{N_1}$ and calculate y_{N_1+2}, y_{N_1+3}, … recursively from Equation 2. Calculate μ_{N_1} as the root of Equation 6 for which $|1 - \mu_{N_1}| < 1$. Alternatively, Equation 7 lets us write $y_{N_1+1} = (1 - \mu_{N_1}) y_{N_1}$ with $|1 - \mu_{N_1}| > 1$.
2. If $g_{N_2} < 0$, take $y_{N_2-1} = (1 - \mu_{N_2-1}) y_{N_2}$ and calculate y_{N_2-2}, y_{N_2-3}, … recursively from Equation 2. With g assumed constant in the right exterior region, μ_{N_2-1} is indistinguishable from μ_{N_2} and can be found from Equation 6 as the root for which $|1 - \mu_{N_2}| > 1$.
3. If $g_{N_2} > 0$, choose an h small enough that $h^2 g_{N_2} < 4$ and take $y_{N_2-1} = \exp(-i\theta_{N_2-1}) y_{N_2}$; then calculate y_{N_2-2}, y_{N_2-3}, … recursively from Equation 2. This models the scattering problem with particles incident from the left to give, in the transmitted region, a solution with a phase that increases with x—that is, a rightward traveling wave. Again, with g constant in the right exterior region, θ_{N_2-1} is indistinguishable from θ_{N_2} and is calculated from Equation 8.

In all cases, the values for y_{N_1} and y_{N_2} are arbitrary, reflecting an overall choice of normalization, and we can set them equal to unity. If steps 1 and 2 both apply, the recursive solutions we obtain must be joined at some intermediate point, say, $n = M$. For optimal visual effect, we first match the slopes at y_M by adjusting the start value y_{N_2}. Then, whenever E is an eigenvalue, both recursions will also give identical values for y_M. Otherwise, the solution is discontinuous at y_M and physically unacceptable. We can find slopes at y_M accurate to $O(h^3)$ using the centered difference

$$y(x_M + h) - y(x_M - h) = 2hy'(x_M) + O(h^3). \quad (9)$$

However, the Numerov implementation is more demanding and requires points two steps removed from x_M to calculate the slopes $y'(x_M)$ to the desired accuracy:

$$y(x_M + h) - y(x_M - h) - (1/8)y(x_M + 2h) + (1/8)y(x_M - 2h) = (3h/2)y'(x_M) + O(h^5). \quad (10)$$

Although convenient, the requirement that g be constant in the exterior regions (these regions must be force free) is unnecessarily restrictive. But if $g(x)$ isn't constant in the exterior regions, Equation 6 affords only approximate values. In this context, we refer to Equation 6 as the *slowly varying approximation* and denote the roots $\tilde{\mu}_n$ to distinguish them from the true values μ_n.

Conventional wisdom dictates that μ_{N_1,N_2-1} be known to an accuracy compatible with the solution technique we use—$O(h^2)$ for the central difference scheme and $O(h^4)$ for the Numerov method. This leads us to ask, how accurate is Equation 6 when the exterior regions aren't force free? An in-depth analysis shows that Equation 6 is justified in principle for calculating μ_n at the endpoints of a suitably large computational interval, provided g_n is asymptotically monotonic and finite valued. (See the "Slowly Varying Approxi-

mation" section for full details.) We can relax the latter restriction to include $g_n \to -\infty$ as $n \to \pm\infty$ (but not $g_n \to +\infty$, which leads to unphysical solution behavior that reflects a fundamental incompatibility between the continuum and discrete asymptotic limits in such cases).

To test the methods in this section, I examined several low-lying stationary states of the quantum oscillator. I performed the calculations in units where $\hbar^2 / 2m = 1$. In these units, the oscillator potential is $V(x) = x^2$, and the allowed energies are the odd integers $E_j = 1, 3, 5, \ldots$. I calculated the waveforms using the central difference approximation on a grid containing 512 points spanning the interval [–5, 5]. For each energy, I generated solutions using discrete transparent boundary conditions applied to each end of the computational interval and matched those solutions near the waveform peak.

Figure 1 shows the results for the three lowest allowed energies. The waveforms in the figure all appear smooth, as expected; by contrast, a discontinuity is already evident in the waveform for $E = 5.005$ (see Figure 2), a value removed from the true energy by just 1 part in 1,000—a 0.1 percent change.

Table 1 reports the fractional mismatch at the match point for each of these waves. The mismatch grows by an order of magnitude with the aforementioned 0.1 percent increase in E over the exact value. For this example, μ_{N_1,N_2-1} should be calculated to accuracy h^2; this requires that the slowly varying approximation $\tilde{\mu}_n$ given by Equation 6 differ from the true value μ_n by no more than $O((10/512)^2) \sim 4 \times 10^{-4}$ at the edges of the computational domain. I refer to the difference $|\mu_n - \tilde{\mu}_n|$ as the *figure of merit*. The last column of Table 1 records the figures of merit estimated from Equation 16; from symmetry, those at the left end of the computational interval ($n = N_1$) are nearly identical and thus omitted. These figures of merit are too large by a factor of five, yet they're still good enough to get the stationary state energies about right.

Although we know that eigenvalues are notoriously insensitive to details of the waveform, calculating other physical quantities might require the extra precision demanded by strictly applying the method. Indeed, we can obtain $O(h^2)$ figures of merit by enlarging the computational interval in this example by a factor of four (while quadrupling the number of points to keep h fixed). Interestingly, the $O(h^4) \sim 10^{-7}$ accuracy the Numerov method demands would require in this example an interval size that's impractically large, which is no doubt because the oscillator potential isn't slowly varying by any realistic measure.

I also checked the applicability of discrete transparent boundary conditions to scattering problems by calculating the probability for particle transmission across a square barrier, another instance in which exact results are available for comparison. Again in units where $\hbar^2 / 2m = 1$, I took the barrier centered at the coordinate origin with unit height and width $w = 4$. This time I calculated the waveforms over the range [–10, +10] using the Numerov scheme on a grid of 2,048 points. At the computational domain's right-side edge, I applied discrete transparent boundary conditions to generate a rightward moving (transmitted) wave in this region.

Figure 3 displays the numerical solution for a particle with energy $E = 0.5$ (half the barrier height). (This waveform is complex valued;conforming to standard practice, color represents the phase of the wave at each point.) The waveform at

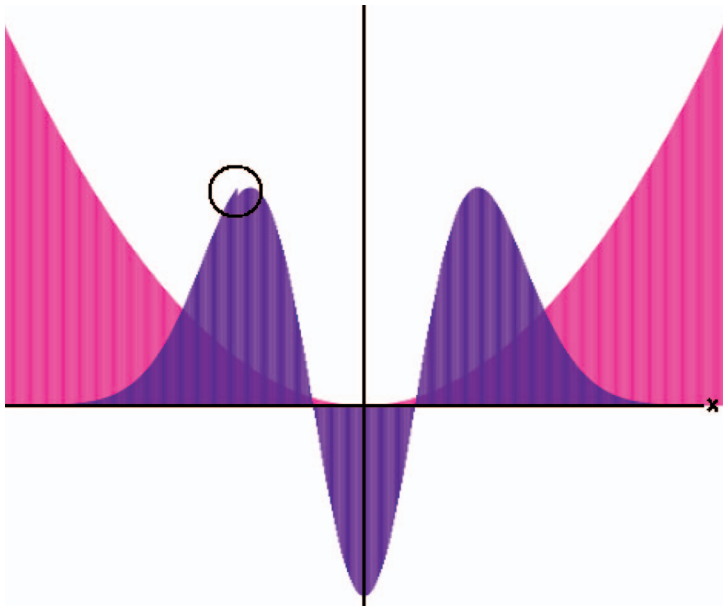

Figure 2. The waveform for the quantum oscillator with $E = 5.005$. The discontinuity in the circled region near the peak on the left indicates this energy isn't one of the allowed values.

Table 1. Characteristics of some numerically generated waveforms for the quantum oscillator.

Energy E	$2\left\lvert\frac{y_M^{(\text{left})} - y_M^{(\text{right})}}{y_M^{(\text{left})} + y_M^{(\text{right})}}\right\rvert$	$\lvert\mu_{N_2-1} - \tilde{\mu}_{N_2-1}\rvert$
1	8.6931×10^{-4}	0.0020
3	2.2554×10^{-3}	0.0022
5	3.9290×10^{-3}	0.0024
5.005	0.03923	0.0024

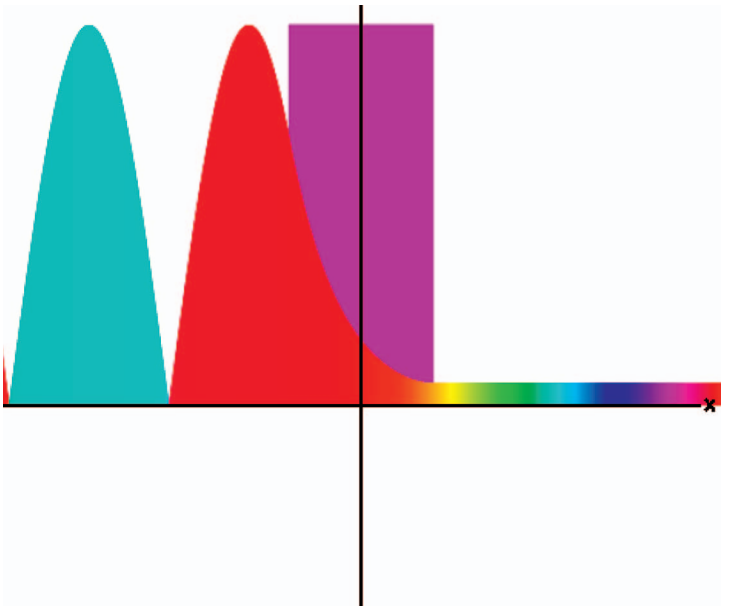

Figure 3. Scattering waveform for a particle incident from the left on a square barrier when the particle energy is one-half the barrier height. The wave is complex valued, with the phase at each point represented by plot color. The wave to the left of the barrier has both incident and reflected components, and the one to the right of the barrier describes pure transmission. The shaded rectangle in the background is the square potential barrier.

the far left is a superposition of incident $y^{(I)}$ (rightward traveling) and reflected $y^{(R)}$ (leftward traveling) waves; sorting out the contribution that each makes to the total is a straightforward exercise in matrix algebra. Noting that $y^{(I)}_{n+1} = \exp(i\theta_n) y^{(I)}_n$ and $y^{(R)}_{n+1} = \exp(-i\theta_n) y^{(R)}_n$, we can write at the left-side endpoint $n = N_1$

$$\begin{pmatrix} y_{N_1} \\ y_{N_1+1} \end{pmatrix} = \begin{pmatrix} 1 & 1 \\ \exp(i\theta_{N_1}) & \exp(-i\theta_{N_1}) \end{pmatrix} \begin{pmatrix} y^{(I)}_{N_1} \\ y^{(R)}_{N_1} \end{pmatrix}.$$

Inverting gives the incident and reflected wave values at N_1:

$$\begin{pmatrix} y^{(I)}_{N_1} \\ y^{(R)}_{N_1} \end{pmatrix} = \frac{1}{2i \sin\theta_{N_1}} \begin{pmatrix} -\exp(-i\theta_{N_1}) & 1 \\ \exp(i\theta_{N_1}) & -1 \end{pmatrix} \begin{pmatrix} y_{N_1} \\ y_{N_1+1} \end{pmatrix}.$$

From these, we calculate transmission (T) and reflection (R) coefficients, respectively, as

$$T = \left| \frac{y_{N_2}}{y^{(I)}_{N_1}} \right|^2 \quad \text{and} \quad R = \left| \frac{y^{(R)}_{N_1}}{y^{(I)}_{N_1}} \right|^2.$$

Any elementary quantum physics text treats particle transmission across a square barrier. In the units I adopted here, the exact result for the transmission coefficient $T(E)$ is conveniently expressed as (for $E < 1$, or below the top of the barrier)[7]

$$\frac{1}{T(E)} = 1 + \frac{1}{4E|1-E|} \sinh^2\left(w\sqrt{|1-E|}\right).$$

This formula remains valid for $E > 1$ (above the barrier) if the hyperbolic sine is replaced by the trigonometric sine. Table 2 compares exact and numerical results for particle transmission at several energies below and above the top of the barrier, including $E = 0.5$ for the waveform of Figure 3. (Because $g(x)$ is constant outside the barrier, figures of merit for slow variation at both edges of the computational domain are zero and, therefore, not tabulated.) T changes by four orders of magnitude over this energy range, yet the agreement between the exact and numerical results is good throughout, with the largest relative error (approximately 1 percent) occurring for the smallest value of T. The right-most column shows the independently calculated value for R added into T; because these are the only outcomes possible in a scattering event, the sum should be unity. The results verify this expectation to 11-digit accuracy and indicate that R is calculated for every energy with a precision that matches T.

Discrete Radial Wave Equation for Spherically Symmetric Potentials

A mass m subject to a central potential $V(r)$ has stationary states of the form $R(r)Y^m_l(\theta, \varphi)$, where (r, θ, φ) are the usual spherical coordinates, Y^m_l denotes the spherical harmonic, and $R(r)$ is the radial wave function. The related function $rR(r)$ satisfies a Schrödinger-like equation with an effective potential that reflects the angular momentum state of the orbiting particle ($l = 0, 1, 2, \ldots$ is the orbital quantum number):

$$V_{eff}(r) = V(r) + \frac{l(l=1)\hbar^2}{2mr^2}. \qquad (11)$$

The machinery developed in the previous sec-

Table 2. Particle transmission across a square barrier.

Energy E	T [exact]	T [calculated]	$T + R$ [calculated]
0.1	7.2849×10^{-4}	7.2044×10^{-4}	1.000000000012
0.3	4.1567×10^{-3}	4.1163×10^{-3}	1.000000000001
0.5	1.3877×10^{-2}	1.3763×10^{-2}	0.999999999998
0.7	4.1302×10^{-2}	4.1041×10^{-2}	0.999999999998
0.9	0.11929	0.11884	1.000000000002
1.2	0.50178	0.50206	0.999999999999
1.5	0.96933	0.97009	0.999999999995
2.0	0.93319	0.93256	1.000000000000
3.0	0.98589	0.98620	0.999999999999
4.0	0.99253	0.99232	1.000000000000

tion also bears on this class of problems. With the identifications $x \to r$, $y(x) \to y(r) = rR(r)$ and $g(x) \to g(r) = 2m[E - V_{eff}(r)]/\hbar^2$, Equation 1 remains the equation of interest, with solutions confined to the domain of the spherical coordinate r—that is, from 0 to ∞. Accordingly, we now take $r \to r_n \equiv nh$ and limit the computational domain to $0 \le n \le N$. We replace the "missing" half axis with the boundary condition $y_0 = 0$, expressing the physical requirement that the radial wave at the origin $R(0)$ must be finite, so $y(r)$ must vanish there. (We must exercise special care with the Numerov method because $y_0 = 0$ doesn't guarantee that $(1 + (h^2/12)g_0)y_0 = 0$ if g_0 is infinite. This is the case for the radial wave equation, where $V_{eff}(r)$ is always singular at the origin for $l > 0$, and even for $l = 0$ is singular for the Coulomb potential and the Yukawa potential, among others. From a numerical perspective, the simplest remedy is to replace g with a model function that differs from the actual one only in having a finite value at the coordinate origin.)

Moreover, y_1 becomes a mere scaling factor that we can take as unity; together with $y_0 = 0$, this is sufficient to obtain from Equation 2 the solution $y_2, y_3, \ldots$ that behaves properly at the origin. Discrete transparent boundary conditions make their appearance at the other end of the computational interval and follow the rules of the preceding section. Specifically, if $g_N < 0$ and g_n is monotonic in the exterior region $n > N$, then a solution with the required accuracy that decays for $r \to \infty$ can be constructed by taking $y_{N-1} = (1 - \mu_{N-1})y_N$, with μ_{N-1} found from Equation 6 and $y_{N-2}, y_{N-3}, \ldots$ calculated recursively using Equation 2. By adjusting the start value y_N, we can match at some intermediate point (r_M) the slope of this decaying solution to the slope of the solution that vanishes at the origin. Any mismatch in the ordinate values at r_M implies that the given energy E isn't allowed.

For the case in which $0 < h^2 g_N < 4$, the large r solutions are oscillatory, and the computational goal switches from locating eigenvalues to extracting partial-wave phase shifts. Starting with $y_0 = 0$ and $y_1 = 1$, we construct the solution $y_2, y_3, \ldots$ from Equation 2 as before. Now, however, the solution at the far right is a mixture of ingoing and outgoing radial waves, which we label $y^{(\text{in})}$ and $y^{(\text{out})}$, respectively. Noting that $y_{n+1}^{(\text{in})} = \exp(-i\theta_n)y_n^{(\text{in})}$ and $y_{n+1}^{(\text{out})} = \exp(i\theta_n)y_n^{(\text{out})}$, where θ_n is given by Equation 8, we can write at the right-side endpoint $n = N$

$$\begin{pmatrix} y_N \\ y_{N-1} \end{pmatrix} = \begin{pmatrix} 1 & 1 \\ \exp(i\theta_{N-1}) & \exp(-i\theta_{N-1}) \end{pmatrix} \begin{pmatrix} y_N^{(\text{in})} \\ y_N^{(\text{out})} \end{pmatrix}.$$

Inverting gives the unique decomposition into ingoing and outgoing waves of the solution that vanishes as required at the origin:

$$\begin{pmatrix} y_N^{(\text{in})} \\ y_N^{(\text{out})} \end{pmatrix} = \frac{1}{2i \sin\theta_{N-1}} \begin{pmatrix} -\exp(-i\theta_{N-1}) & 1 \\ \exp(i\theta_{N-1}) & -1 \end{pmatrix} \begin{pmatrix} y_N \\ y_{N-1} \end{pmatrix}.$$

Because y_N and y_{N-1} must be real, we find that $y_N^{(\text{in})*} = y_N^{(\text{out})}$; the solution in the outer region is an equal mix of ingoing and outgoing waves—that is, a *standing wave*. The quantity of interest is the phase of this standing wave, $\chi = \arg(y_N^{(\text{out})})$. With the help of Equation 8, we can write this as

$$\chi = \arctan\left[\frac{y_{N-1} - y_N \cos\theta_{N-1}}{y_N \sin\theta_{N-1}}\right] = \arctan\left[\frac{h^2 g_{N-1} - 2\dfrac{\Delta y_{N-1}}{y_N}}{\sqrt{4h^2 g_{N-1} - h^4 g_{N-1}^2}}\right]. \quad (12)$$

Table 3. Some *S*-wave phase shifts for the spherical well.

Energy E	$\delta_0(E)$ [exact]	$\delta_0(E)$ [calculated]
0.1	–0.77748	–0.77849
0.5	–0.9416	–0.94348
1.0	–1.3313	–1.3316
5.0	0.82377	0.82370
10	0.59401	0.59383

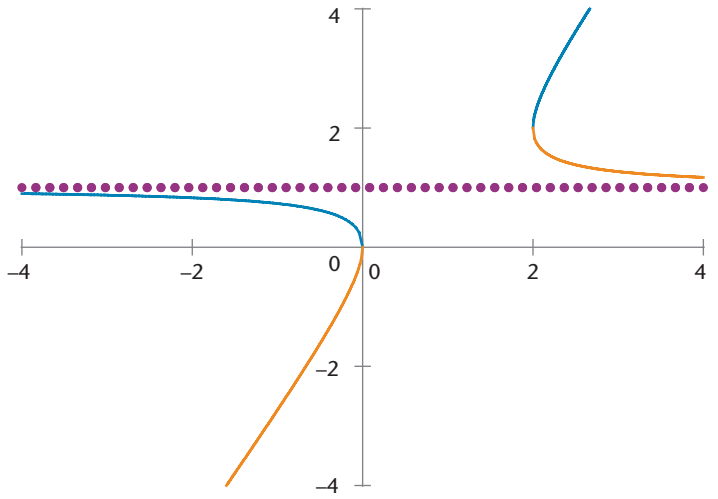

Figure 4. The variation of μ (ordinate values) from Equation 6 with the (assumed continuous) variable $h^2g_n/2$. The branch μ^+ takes the largest values in each of the plot intervals and is green; the μ^- branch is brown. The horizontal asymptote at $\mu = 1$ is approached from below by μ^+ as $g_n \to -\infty$ and from above by μ^- as $g_n \to +\infty$. The range $h^2g_n/2 > 2$ isn't physical, but I include it here for completeness.

Finally, we find the phase shift for the lth partial wave δ_l by comparing this phase with the corresponding free particle result obtained by taking $V(r) = 0$ in the effective potential of Equation 11: specifically, $\delta_l = \chi - \chi_{(V=0)}$.

Table 3 compares $l = 0$ (S-wave) phase shifts at several different energies calculated using Equation 12 with exact results for the spherical well. Again in units where $\hbar^2 / 2m = 1$, I took the well to have unit depth and radius $a = 4$. Exact values for this case are well known. In the units I adopted here, S-wave phase shifts for the spherical well[8] are given by

$$\delta_0(E) = \arctan\left(\frac{\sqrt{E}\tan(a\sqrt{E+1})}{-\sqrt{E+1}\tan(a\sqrt{E}) \Big/ \sqrt{E+1} + \sqrt{E}\tan(a\sqrt{E+1})\tan(a\sqrt{E})}\right). \quad (13)$$

The numerical results agree well with the exact values of Equation 13 over the whole range of energies I studied. In this example, the largest error (approximately 0.2 percent) occurred for the intermediate value $E = 0.5$, followed closely by the ~0.13 percent discrepancy observed for the smallest energy in this sample.

Slowly Varying Approximation

This section investigates the validity of Equation 6 in exterior regions that aren't force free. Because the arguments I present here are technical and of limited interest, the casual reader might want to skip them entirely.

Let's return to Equation 2 and let $\tilde{y}$ denote the solution obtained using some trial $\tilde{g}$ that differs from the actual g in the region of interest. We limit our remarks to the right exterior region $n > N_2$; analogous arguments apply to the left exterior region $n < N_1$. We assume that $\tilde{y}$ and y satisfy identical boundary conditions at infinity so that $\tilde{y}$ coincides with the exact solution when $\tilde{g} \to g$. Now use the identity

$$y_n\Delta^2\tilde{y}_{n-1} - \tilde{y}_n\Delta^2 y_{n-1} \equiv \Delta(y_n\Delta\tilde{y}_{n-1} - y_n\Delta\tilde{y}_{n-1})$$

together with Equation 2 to write

$$\Delta(y_n\Delta\tilde{y}_{n-1} - \tilde{y}_n\Delta y_{n-1}) = \Delta[y_n\tilde{y}_n(\tilde{\mu}_{n-1} - \mu_{n-1})] = h^2(g_n - \tilde{g}_n)y_n\tilde{y}_n.$$

For the right-side exterior, we sum this result from N_2 to ∞ and assume $\lim_{n\to\infty} y_n\tilde{y}_n(\tilde{\mu}_{n-1} - \mu_{n-1})$ vanishes to get (with $y_{N_2} = \tilde{y}_{N_2} = 1$):

$$\mu_{N_2-1} - \tilde{\mu}_{N_2-1} = h^2 \sum_{n=N_2}^{\infty} (g_n - \tilde{g}_n)y_n\tilde{y}_n \ .$$

In the slowly varying approximation we take $h^2\tilde{g}_n + \Delta\tilde{\mu}_{n-1} = h^2 g_n$; then $\tilde{\mu}_n$ is given *exactly* by Equation 6 (with g_n not $\tilde{g}_n$, see Equation 5) and

$$\mu_{N_2-1} - \tilde{\mu}_{N_2-1} = \sum_{n=N_2}^{\infty} \Delta\tilde{\mu}_{n-1}y_n\tilde{y}_n \,. \quad (14)$$

To be consistent, the sum on the right of Equation 14 should converge to a function that vanishes as $N_2 \to \infty$. Then for a given value of h, we can, in principle, always find an N_2 large enough to make the right side $O(h^2)$ for central difference calculations and $O(h^4)$ for Numerov work. Our goal, therefore,

is to establish the best possible upper bound for this sum. To that end, recall that the exact solution y_n is bounded; accordingly, we assume subsequently that N_2 has been chosen to make $|y_n| \le y_{N_2} = 1$ for all $n \ge N_2$. Also, the definition of $\tilde{\mu}$ implies that we can write $\tilde{y}_n = (1-\tilde{\mu}_{n-1})(1-\tilde{\mu}_{n-2}) \cdots (1-\tilde{\mu}_{N_2})\tilde{y}_{N_2}$, whereas Equation 6 requires $|1-\tilde{\mu}| \le 1$ for each of the $n - N_2$ factors.

Consider first the case in which $g_n < 0$ (or $h^2 g_n > 4$). If g_n is monotonic for $n \ge N_2$, then both branches in Equation 6 define roots $\tilde{\mu}_n$ that are real and also monotonic for $n \ge N_2$. In fact, both $\Delta\tilde{\mu}_{n-1}$ and $\tilde{\mu}_n$ are monotonic with g_n (see Figure 4). Moreover, $\lim_{n\to\infty}\tilde{\mu}_n$ exists if $\lim_{n\to\infty} g_n$ also exists, but even if g_n diverges for $n \to \infty$, we find $\lim_{n\to\infty}\tilde{\mu}_n = 1$ for the root of interest (the one for which $|1-\tilde{\mu}| \le 1$). In either case, $\lim_{n\to\infty}\Delta\tilde{\mu}_{n-1} = 0$, and Equation 14 is bounded above by

$$\left|\mu_{N_2-1} - \tilde{\mu}_{N_2-1}\right| \le \left|\Delta\tilde{\mu}_{N_2-1}\right| \sum_{n=N_2}^{\infty} \left|1-\tilde{\mu}_{N_2}\right|^{n-N_2} = \left|\frac{\Delta\tilde{\mu}_{N_2-1}}{1-|1-\mu_{N_2}|}\right|. \quad (15)$$

The simple bound Equation 15 is adequate to ensure that $\tilde{\mu}_{N_2-1}$ differs from the exact value μ_{N_2-1} by an arbitrarily small amount for large enough values of N_2, but it might be too crude for the more exacting task of deciding when the computational interval is large enough. We can obtain a somewhat better estimate (although not a strict upper bound) by replacing y_n on the right side of Equation 14 with $\tilde{y}_n$; this gives

$$\left|\mu_{N_2-1} - \tilde{\mu}_{N_2-1}\right| \lesssim \left|\frac{\Delta\tilde{\mu}_{N_2-1}}{1-(1-\tilde{\mu}_{N_2})^2}\right| = \left|\frac{\Delta\tilde{\mu}_{N_2-1}}{\tilde{\mu}_{N_2}(2-\tilde{\mu}_{N_2})}\right|. \quad (16)$$

No better general estimates are likely in this case; indeed, if we believe only that y_n has the same sign as $\tilde{y}_n$ for all $n \ge N_2$, then the monotonic behavior of g_n guarantees that all terms in Equation 14 are cumulative, so the sum's magnitude exceeds that of any one term. In particular, we can expect $|\mu_{N_2-1} - \tilde{\mu}_{N_2-1}| > |\Delta\tilde{\mu}_{N_2-1}|$.

Similar reasoning applies to the oscillatory case $0 < h^2 g_n < 4$, but now $\tilde{\mu}_n$ is complex with real and imaginary parts that we must handle separately. Using Equation 6, we have in place of Equation 1,

$$\mu_{N_2-1} - \tilde{\mu}_{N_2-1} = \frac{h^2}{2}\sum_{n=N_2}^{\infty} \Delta g_{n-1} y_n \tilde{y}_n \pm \frac{i}{2}\sum_{n=N_2}^{\infty} \Delta\left(\sqrt{4h^2 g_{n-1} - h^4 g_{n-1}^2}\right) y_n \tilde{y}_n \ .$$

The radical increases with g_n for $h^2 g_n < 2$ and decreases for $2 < h^2 g_n < 4$. In the simplest scenario, one or the other inequality holds throughout the exterior region $n \ge N_2$, with the consequence that the sums on the right are bounded by

$$\left|\sum_{n=N_2}^{\infty} \Delta g_{n-1} y_n \tilde{y}_n\right| \le \sum_{n=N_2}^{\infty} \left|\Delta g_{n-1}\right| = \left|g_\infty - g_{N_2-1}\right|$$

$$\left|\sum_{n=N_2}^{\infty} \Delta\left(\sqrt{4h^2 g_{n-1} - h^4 g_{n-1}^2}\right) y_n \tilde{y}_n\right| \le \left|\sqrt{4h^2 g_\infty - h^4 g_\infty^2} - \sqrt{4h^2 g_{N_2-1}^2 - h^4 g_{N_2-1}^2}\right|$$

assuming g_n is monotonic for $n \ge N_2$. Straightforward modifications are required if the exterior region includes the crossover point $h^2 g_n = 2$. Taken together, these results again ensure that $\tilde{\mu}_{N_2-1}$ differs from the exact value by an arbitrarily small amount provided N_2 is sufficiently large.

If the oscillatory case applies for all $n \ge N_2$, then $\lim_{n\to\infty} g_n \equiv g_\infty$ must exist. If this limit doesn't exist—if g_n diverges as $n \to \infty$—then the exterior region includes a critical point N_c (not necessarily integer) defined by $h^2 g_{N_c} = 4$ and the estimate of Equation 15 applies for $N_2 \ge N_c$. But $\tilde{y}_n$ oscillates wildly for $n \ge N_c$ (because $\tilde{\mu} > 1$ for $h^2 g_n > 4$, $\tilde{y}_n$ and $\tilde{y}_{n+1}$ have opposite sign) and bears no apparent relation to the discretized version of the continuum solution in this range. This unphysical behavior isn't a failure of the slowly varying approximation; it stems from the inability of any discrete form on a uniform mesh to follow a continuum solution that oscillates with ever-increasing rapidity. Evidently, the continuum limit $h \to 0$ is incompatible with the discrete asymptotic limit $n \to \infty$ in such cases. (A similar circumstance arises with the Numerov method if $g_n < 0$ and is unbounded for $n \to \infty$. The Numerov renormalized value (see Equation 4) becomes singular for that N_s (not necessarily integer) that makes $1 + h^2/12 g_{N_s} = 0$ and changes sign for $n > N_s$, passing through the critical point N_c to eventually saturate at the value $12/h^2$. Again, the behavior of $\tilde{y}_n$ (and y_n) is decidedly unphysical for $n \ge N_s$.). The dilemma is resolved in practice by replacing g_n with a constant in the asymptotic region $n \gtrsim N_c$, thereby render-

ing $\Delta\tilde{\mu}_{n-1} \equiv 0$ there and truncating the sum in Equation 14 at some $N < N_c$. In effect, we first cap the troublesome divergence at the continuum level and then discretize the resulting model.

Hence, so long as g_n is asymptotically monotonic, the slowly varying approximation of Equation 6 can—at least, in principle—be used to generate solutions to centered-difference or Numerov accuracy by adopting a suitably large computational interval.

In this article, I advocate using discrete transparent boundary conditions to solve eigenvalue problems, notably those posed by the stationary state Schrödinger equations of quantum mechanics. The methods I outline here for calculating allowed particle energies, scattering coefficients, and partial wave phase shifts are used extensively in a software application, QMTools, that I authored to help beginning students visualize the abstract concepts of quantum physics. Visit the QMTools project Web site http://people.uncw.edu/moyerc/QMTools/ to download the software along with numerous examples illustrating its pedagogical benefits. CiSE

Acknowledgment

The US National Science Foundation, under grant number DUE-9972322, provided financial assistance for this project.

References

1. P.C. Chow, "Computer Solutions to the Schrödinger Equation," *American J. Physics*, vol. 40, no. 5, 1972, pp. 730–734.
2. J.L.M. Quiroz Gonzalez and D. Thompson, "Getting Started with Numerov's Method," *Computers in Physics*, vol. 11, no. 5, 1997, pp. 514–515.
3. A. Arnold, "Numerically Absorbing Boundary Conditions for Quantum Evolution Equations," *VLSI Design*, vol. 6, 1998, pp. 313–319.
4. M. Ehrhardt, "Discrete Transparent Boundary Conditions for General Schrödinger-Type Equations," *VLSI Design*, vol. 9, no. 4, 1999, pp. 325–338.
5. C.A. Moyer, "Numerov Extension of Transparent Boundary Conditions for the Schrödinger Equation in One Dimension," *American J. Physics*, vol. 72, no. 3, 2004, pp. 351–358.
6. J.V. Noble, "The Right Angle: Precise Numerical Orthogonality in Eigenstates," *Computing in Science & Eng.*, vol. 4, no. 5, 2002, pp. 91–97.
7. R. Serway, C. Moses, and C. Moyer, *Modern Physics*, 3rd ed., Brooks/Cole-Thomson Learning, 2005.
8. S. Gasiorowicz, *Quantum Physics*, 2nd ed., John Wiley & Sons, 1996.

Curt A. Moyer *is professor and chair of the Department of Physics and Physical Oceanography at the University of North Carolina, Wilmington. His research interests include ion-surface collisions, properties of matter in superstrong fields, and physics pedagogy. Moyer has a PhD in physics from the State University of New York at Stony Brook. He is a member of the American Physical Society, the American Association of Physics Teachers, Phi Beta Kappa, and the Society of Sigma Xi. Contact him at moyerc@uncw.edu.*